THE JOURNAL OF PHYSICAL CHEMISTRY LETTERS
A JOURNAL OF THE AMERICAN CHEMICAL SOCIETY

pubs.acs.org/JPCL

Letter

Evidence for Field-Dependent Charge Separation Caused by Mixed Phases in Polymer–Fullerene Organic Solar Cells

Prabodh Dhakal, Thomas Ferron, Awwad Alotaibi, Victor Murcia, Obaid Alqahtani, and Brian A. Collins*

Cite This: *J. Phys. Chem. Lett.* 2021, 12, 1847–1853

Read Online

ACCESS | Metrics & More | Article Recommendations | Supporting Information

ABSTRACT: As organic photovoltaic performance approaches 20% efficiencies, causal structure–performance relationships must be established for devices to realize theoretical limits and become commercially competitive. Here, we reveal evidence of a causal relationship between mixed donor–acceptor interfaces and charge generation in polymer–fullerene solar cells. To do this, we combine a holistic loss analysis of device performance with quantitative synchrotron X-ray nanocharacterization to identify a >98% anticorrelation between field-dependent geminate recombination and nanodomain purity. Importantly, our analysis eliminates other possible explanations of the performance trends, a requirement to establish causality. The unprecedented granular level of our analysis also separates field-dependent and field-independent recombination at the interface, where we find for the first time that this system is free of field-independent recombination, a loss channel that plagues high-performance systems, including those with non-fullerene acceptors. This result broadens the case that minimizing mixed phases to promote sharp interfaces between pure aggregated domains is the ideal nanostructure for realizing theoretical efficiency limits of organic photovoltaics.

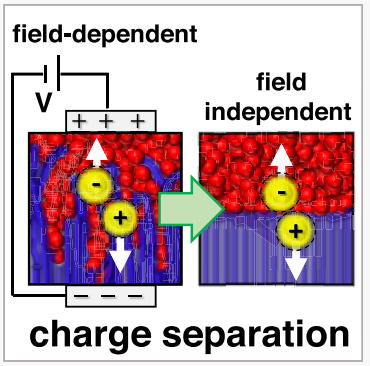

Organic photovoltaic devices (OPVs) have great potential for the generation of solar power from earth abundant, nontoxic, and flexible materials that could be massively scaled beyond current technologies using roll-to-roll printing infrastructure. The best power conversion efficiencies (PCEs) are 18%,[1,2] but to realize their potential, increasing the PCE to >20% is necessary. As theoretical limits of performance are approached, it is increasingly necessary to quantify each loss at a more detailed level to precisely identify and eliminate the remaining losses.

One primary focus is the morphology of the electron donor–acceptor interface where charge generation occurs from the initial photoexcited excitons. In particular, molecularly mixed interfaces versus interfaces between ordered, crystalline phases have been debated in terms of which is more beneficial to devices. Mixed phases possess a superior interfacial area and an energy gradient,[3−5] while sharp interfaces between pure phases could exhibit a higher separation efficiency due to delocalization of interfacial states.[6,7] Increased phase purity has been recently linked to increased device fill factors for amorphous polymer–fullerene systems,[8] but what fundamental dynamics underlies this performance is uncertain: enhanced charge generation (reduced geminate recombination) or increased charge extraction (reduced bimolecular recombination). Many studies focus on charge transport to probe extraction, measuring the order and rate of bimolecular recombination,[9] while others examine the dynamics of charge generation.[10] Although correlations can be found in both cases, it is difficult to simultaneously quantify the impact of both of these processes on performance to determine which is the main influence, dictating the highest potential for performance gains. In particular, ultrafast spectroscopies have advanced considerably to simultaneously probe the time scales of both generation and recombination.[11,12] However, these studies depend on extremely high fluences and are not applied to devices. Thus, a comparison of the impact of geminate versus bimolecular recombination on device performance cannot be assessed; in particular, the field dependence on such dynamics is not studied.

Recently, we demonstrated a new analytical technique for separately quantifying each loss mechanism in an OPV under operating fields.[13] Through such a holistic analysis, we revealed in P3HT:PCBM OPVs evidence for a causal relationship between sharp interfaces and CT state separation efficiency at those interfaces that governed device performance. Combined with previous studies of amorphous systems,[8] this suggests that a high phase purity is desirable in both amorphous and highly crystalline systems. However, P3HT:$PC_{61}BM$ is a relatively low-performance system and exhibits a crystalline packing that

Received: January 2, 2021
Accepted: February 5, 2021
Published: February 12, 2021

is much stronger than most high-performing systems. Thus, it is of interest to explore whether a moderately ordered system with higher performance also exhibits these trends of increased charge generation with phase purity.

In this work, we characterize the losses of PCPDTBT:$PC_{71}BM$ bulk heterojunction OPVs as a function of diiodooctane (DIO) processing additive (molecular structures shown in the inset of Figure 1a). This is a good

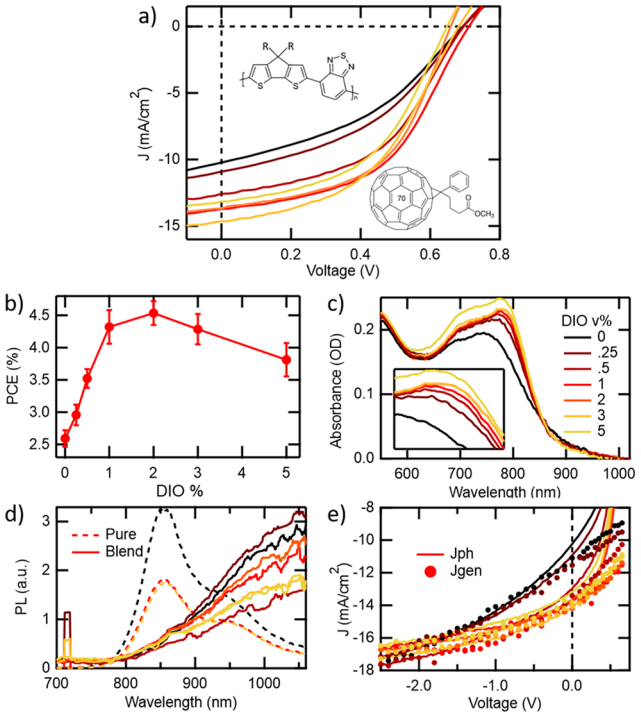

Figure 1. Device performance and fundamental properties. (a) JV device characteristics under AM1.5G illumination. Molecular structures are shown in the inset. R = ethylhexyl. (b) Power conversion efficiency (PCE) extracted from panel a as a function of DIO volume percent of the processing solvent. Uncertainty bars are the standard deviations of four devices on a single substrate. (c) Absorbance spectra of active layers just between the tested devices. The inset is a close-up of the aggregate absorbance. (d) Photoluminescence (PL) spectra of both pure polymer and blend films. An excitation wavelength of 600 nm balances absorbance between the polymer and fullerene. Blend film signals are amplified 100-fold compared to those of the pure films. (e) Photocurrent density $J_{ph} = J_L - J_D$ (solid lines), where J_L is the current density under 1 sun illumination and J_D is the device current density in the dark. Generated current J_{gen} (dotted lines) as a function of bias voltage during generation for each sample as measured from TDCF.

model system because its performance is higher and the system is less crystalline than P3HT:PCBM, but also a well-investigated, model system. This system is also interesting because it exhibits field-dependent geminate recombination (charge generation that depends on the applied voltage).[14,15] This contrasts with P3HT:PCBM cells whose geminate recombination is field-independent and therefore uses a different mechanism.[13,16] These two geminate recombination mechanisms have not been quantified in a single system before but must be explored to understand and eliminate both loss channels. Furthermore, the losses quantified in PCPDTBT:PCBM cells have thus far been only qualitatively associated with increased phase separation afforded by an additive.[12,17,18] However, it has not been established whether the additive effect is due to increased crystallinity or increased phase purity, two parameters that are difficult to dissentangle but can nonetheless affect device dyanmics in different ways. A much more deterministic and quantitative link to one or the other is required to drive the design of materials.

In our detailed loss analysis of PCPDTBT:$PC_{71}BM$ devices, we reveal for the first time that no field-independent recombination exists at all in these devices, a phenomenon that will be important for achieving theoretical limits of device efficiency. We also confirm that field-dependent geminate recombination is the main loss mechanism in optimized devices with bimolecular recombination playing only a minor role under the operating conditions. We combine advanced synchrotron X-ray probes to fully characterize the nanostructure and ordering within devices. This analysis reveals that geminate recombination is tied primarily to phase purity with an impressive 98% Pearson correlation through the DIO series. While data show that aggregation is clearly important, the crystal or aggregate population or coherence does not correlate with performance in key ways that uniquely allow us to separate these effects from domain purity. This strengthens the evidence of a causal structure−property relationship. Such a result adds to the growing body of evidence that sharp interfaces between pure, aggregated domains are the most desirable morphology for the highest charge separation yields and best device efficiencies.

Panels a and b of Figure 1 present JV characteristics and their power conversion efficiency (PCE) under AM1.5G solar illumination. All metrics can be found in SI Note 1, all of which closely follow previous reports.[15,19] The highest-performing devices in our series were cast from 2 vol % DIO, and most of the performance boost was seen by 1 vol % DIO. The fill factor decreased the performance at DIO concentrations beyond 2 vol %. Absorbance spectroscopy data acquired on the actual devices are shown in Figure 1c and reveal all active layers were approximately the same thickness (~130 nm). Similar to other studies,[17] the DIO additive increases the intensity of the polymer aggregation peak at 780 nm (see the inset of Figure 1c). Most of the increase occurs by 0.25% DIO, earlier than the increase in performance. The aggregation peak continues to grow through the end of the series, consistent with DIO's effect as a plasticizer but again inconsistent with performance trends. Thus, to understand the origins of these trends, a more in-depth characterization of the generation−recombination process is required.

Photoluminescence quenching experiments were conducted on identically prepared active layers and pure polymer films (Figure 1d) to quantify excitonic losses. The pure films reveal typical excitonic emission from PCPDTBT,[20] and when cast using a DIO additive, the emission efficiency decreases. No sign of excitonic emission can be detected in any of the blends, however. Instead, the much-amplified blend spectra are consistent with that of the weak CT state emission.[14] The complete quenching of exciton emission (>99%) agrees with previous reports using transient absorption[12] and indicates all excitons arrive at an interface with the fullerene, eliminating this typical loss channel for all levels of DIO in our series.

To disentangle geminate and bimolecular losses, time-delayed collection field (TDCF) measurements of generation current J_{gen} are calculated similar to previous reports[13,17] and are compared with photocurrent (J_{ph}) at 1 sun in Figure 1e. Special experimental conditions (see Methods) ensured

https://dx.doi.org/10.1021/acs.jpclett.0c03863
J. Phys. Chem. Lett. 2021, 12, 1847−1853

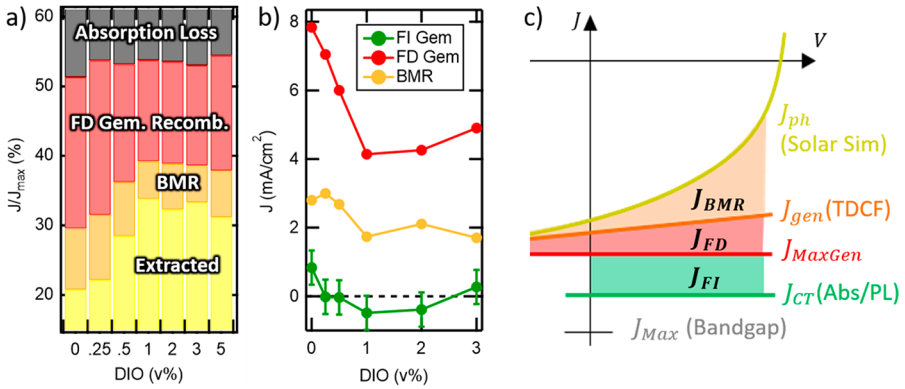

Figure 2. Quantitative OPV loss analysis. (a) Composite figure of current density at each step in the generation processes as a percentage of the total possible, considering the experimentally resolved polymer band gap of 835 nm. Values are for the device held at the maximum power point. Losses are from the failure to absorb a photon (gray, extending to 100%), excitons failing to find an interface (none in this system), field-dependent geminate recombination of CT states (red), and bimolecular recombination of separated charges (BMR, orange). The yellow region represents the extracted charge. (b) Quantified photocurrent density losses from field-independent (FI) and field-dependent (FD) geminate recombination as well as bimolecular recombination (BMR). Uncertainty bars are from the estimated uncertainty in absorbance loss calculations and standard deviation of TDCF measurements. (c) Schematic of how each loss current density is calculated and related to current densities at each step in the analysis. See SI Notes 2–4 for all details.

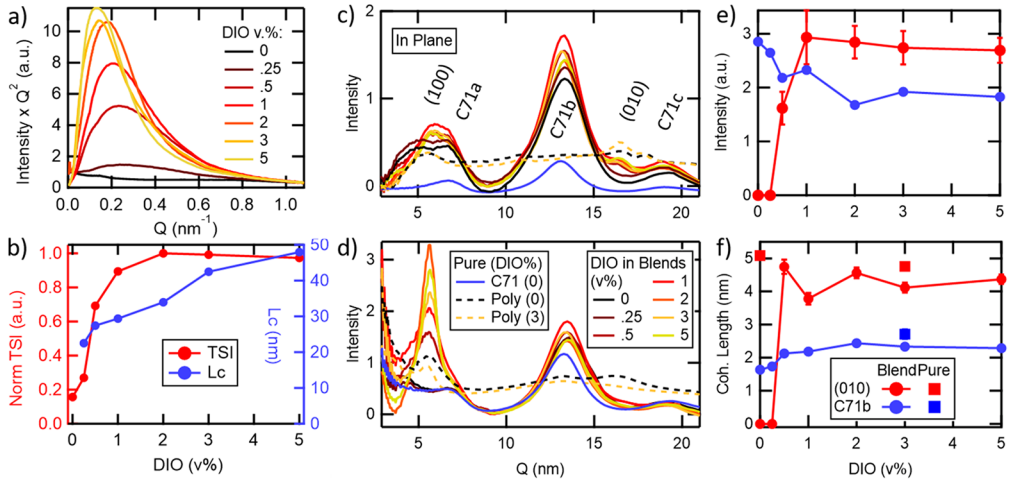

Figure 3. Analysis of active layer morphology. (a) RSoXS scattering profiles at 283.5 eV (just below the absorbance edge) plotted as Lorentz-corrected to emphasize total scattering intensity (TSI) and the location of the scattering feature due to lateral domain structure. (b) TSI and characteristic length $L_C = 2\pi/q^*$ as a function of DIO solvent additive concentration. q^* is taken as the maximum in the scattering profiles in panel a. (c) In-plane and (d) out-of-plane GIWAXS scattering profiles for pure and blend films. Pure polymer films are offset in intensity for the sake of clarity. Diffraction peaks are labeled for the polymer crystal direction [(100) lamellar and (010) π-stacking] or for fullerene scattering C71a, C71b, and C71c in order of q position. (e) Integrated peak intensity (red) for the polymer π-stacking (010) and (blue) for the dominant fullerene scattering peak (C71b) in blend active layers. (f) Scherrer analysis of the crystal coherence length ($L_{coh} = 0.94 \times 2\pi/\text{fwhm}$) for the same two features in panel e as well as for pure films of each component. Uncertainty bars are shown for all data in panels e and f from peak fitting. Details of raw data processing and peak analysis can be found in SI Note 5.

accurate measurement of charge generation.[21] At most reverse biases, $J_{ph} \cong J_{gen}$, indicating field-dependent geminate recombination dominates bimolecular recombination. At positive generation biases, however, the two currents diverge as bimolecular recombination becomes important. This field-dependent bimolecular recombination is likely due to the limited mobility of the polymer, causing separation between and gradients in the quasi Fermi levels.[22] In general, the addition of DIO aids in increasing J_{gen} at operational (positive) biases in agreement with previous reports.[15,17] Such behavior is very different from that of P3HT:PCBM, which exhibits only field-independent geminate recombination.

It is established that the DIO additive affects the active layer morphology of many systems to reduce both geminate and bimolecular recombination. Which loss mechanism is more important for device performance, however, is often unknown, because geminate and bimolecular recombinations are rarely measured in a way that can be directly compared. We quantify and compare these directly in Figure 2 using our previously reported analysis that quantifies each loss process as an effective photocurrent.[13] At 13–22% of all photons lost (Figure 2a) or 4–8 mA/cm^2 lost (Figure 2b), geminate recombination is by far the main charge loss in this system compared with 6–8% photons or 2–3 mA/cm^2 from bimolecular losses at the maximum power point. At short circuit, geminate recombination is even more dominant (see Figure S4). While the effects of the DIO additive decreased

https://dx.doi.org/10.1021/acs.jpclett.0c03863
J. Phys. Chem. Lett. 2021, 12, 1847–1853

both losses, it impacts geminate recombination more substantially.

Importantly, our analysis quantifies both field-dependent (FD) and field-independent (FI) geminate loss channels separately and is described schematically in Figure 2c. As detailed previously,[13] the FI losses are calculated from the difference between J_{CT} (current density of CT states produced) and J_{MaxGen} (maximum generation current that can be attained by a field). J_{CT} is calculated by subtracting absorption losses (using transfer matrix methods[23]) and excitonic (PL) losses from J_{max} based on the polymer bandgap (see the Supporting Information for our detailed calculations). J_{MaxGen} is calculated from the saturated photocurrent at a high reverse bias under 1 sun conditions. In another surprise, within uncertainty $J_{MaxGen} = J_{CT}$, meaning with a sufficiently high field, all CT states are successfully separated, and there is no measurable FI geminate recombination in this system for any level of DIO ($J_{FI} = 0$ for all cells, except possibly at 0% DIO). This situation is the opposite from that of P3HT, where there is only FI recombination that does vary with processing conditions. Such a result suggests multiple possible mechanisms for geminate recombination at the donor−acceptor interface, the origin of which deserves further study, in particular because even high-performing non-fullerene acceptor (NFA) systems exhibit FI geminate recombination.[24] As this is the first time a complete absence of FI geminate recombination has been identified for any OPV system, this system may be key to understanding how to eliminate this loss channel in high-performing NFA systems.

To investigate the morphological origins of the changing device performance and underlying dynamics, we conducted both resonant soft X-ray scattering (RSoXS) and grazing incidence wide-angle X-ray scattering (GIWAXS) on the active layers. RSoXS scattering profiles (Figure 3a) are analyzed in Figure 3b, which at resonance emphasizes lateral fluctuations in molecular composition (donor−acceptor domains). The RSoXS total scattering intensity (TSI) is proportional to domain purity, while the characteristic length (L_c) is proportional to domain size and spacing.[25] The trends reveal a homogeneous blend without DIO, which immediately develops phase-separated domains with even the lowest DIO concentration (0.25 vol %). The phase purity plateaus with 2 vol % DIO, while the domain size increases continuously with DIO, consistent with Oswald domain ripening after initial compositional phase separation. However, the characteristic length never grows past 50 nm in the range of DIO concentrations investigated, potentially explaining why no appreciable exciton recombination (exciton PL) is detected despite relatively pure domains.

In-plane and out-of-plane GIWAXS scattering profiles are displayed in panels c and d of Figure 3, respectively, for all investigated samples. For the blends, there is enhanced π-stacking (010) in plane and lamellar stacking (100) out of plane, indicating an edge-on preference for polymer crystals. Diffraction intensity (Figure 3e) and coherence length (Figure 3f) from peak fits of the in-plane polymer π-stacking and primary fullerene peaks are displayed as a function of DIO concentration. For blend films cast with no DIO and 0.25 vol % DIO, there is no sign of π-stacking at all (any orientation), while the intensity and coherence length of π-stacking essentially turn on at 0.5 vol % DIO and mimic pure films without significant evolution. This is remarkable as such a trend does not track with performance (a monotonic increase to 2 vol % and then a slight decrease) or recombination currents. The fullerene packing peak also does not evolve significantly in the DIO series. The coherence length being similar with that of pure fullerene films indicates pure fullerene domains exist as one phase in the blend as is typical with polymer fullerene blends.

The combined ultraviolet−visible (UV−vis), RSoXS, and GIWAXS measurements reveal an optimized active layer that consists of a polymer phase composed nominally of pure crystallites, tens of nanometers in size, surrounded by a pure fullerene matrix in agreement with previous characterizations.[26] Our unique gradual variation of DIO enables us to generate a picture of film formation where DIO plasticizes the initially fully mixed and disaggregated layer. First, DIO enables intramolecular polymer aggregation (by 0.25 vol % DIO), then intermolecular packing (at 0.5 vol % DIO), then further domain purification (through 2 vol % DIO), and finally domain size ripening (at higher DIO concentrations). Importantly, the aggregation and crystallinity trends do not increase in a way that mirrors performance. Only domain purity mirrors performance and is thus the most likely morphological cause of the performance trends. Increasing purity without increasing polymer crystallinity can mean either increasingly clustered polymer crystallites within the polymer-rich phase (reducing the fullerene between crystals) or increasingly narrow (smaller) mixed phases between polymer crystallites and pure fullerene aggregate phases. The latter of these possibilities has been confirmed for P3HT:PCBM blends via energy-filtered electron microscopy,[27] but not for PCPDTBT:PCBM blends.

The FD geminate recombination follows the performance trends above all other loss processes. Figure 4a displays the fate of CT states at the maximum power point. Here the trend in FD geminate recombination strongly anticorrelates with the percent extracted charge (internal quantum efficiency), while the bimolecular recombination hardly changes at all through the series, hovering around 14(3)%. Although previous studies have found that additives reduce the bimolecular recombination coefficient in PCPDTBT blends,[12] such knowledge is insufficient to assess the impact on devices as charge density (increasing due to smaller geminate losses) impacts bimolecular recombination just as strongly. From our analysis, we find that these two contributions to bimolecular recombination work against each other to limit the final effect on device performance. This direct comparison of the performance impact of these two loss channels is a missing component of many OPV analyses and will be critical to identify the true limits of a material system or a processing strategy.

As both phase purity and FD geminate recombination correlate with device performance, it makes sense that they would be connected to each other. Figure 4b demonstrates this connection by plotting normalized phase purity with geminate photocurrent losses as a function of DIO concentration. They follow each other quite closely. Establishing causality, however, is a particularly important goal, because too many OPV morphological and device parameters often follow each other, making it difficult to target and modify the actual limiting properties. The correlation analysis between these two parameters in Figure 4c reveals a 98% Pearson correlation. Such a high correlation is the first step toward establishing causality. The second step is eliminating other possibilities (such as the aggregation and crystallinity or other loss

https://dx.doi.org/10.1021/acs.jpclett.0c03863
J. Phys. Chem. Lett. 2021, 12, 1847−1853

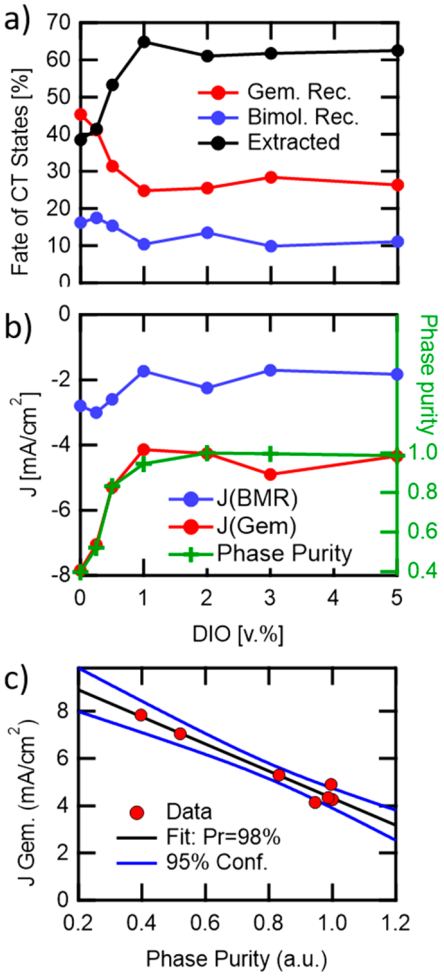

Figure 4. Geminate recombination correlates with phase purity. (a) Quantitative fate of all CT states as a percentage of the total CT state generated at the maximum power point. (b) Photon current losses (left axis) plotted with phase purity ($P \propto \sqrt{\mathrm{TSI}}$, right axis). (c) Correlation analysis of geminate recombination current connects to phase purity with 95% confidence intervals shown. The Pearson correlation is 98%.

processes), which we also have done here. The final proof of causality requires establishing time order, which we were unable to do in this study, yet still leaves strong evidence of a causal relationship.

A causal relationship between domain purity and geminate recombination is similar to our previous finding in P3HT:PCBM cells,[13] but the FD loss mechanism in this system is different from the FI loss mechanism in P3HT. This broadens the case that pure domains are crucial for the high efficiency of charge generation in semicrystalline polymer–fullerene OPVs regardless of the loss mechanism. A previous study of pBTTT-C_{16}:$PC_{61}BM$ blends involving a bimolecular crystal of the two molecules (representing a mixed phase) indicated that pure fullerene phases are necessary to smaller FD geminate losses in agreement with our result here.[28] In that study, however, neither excitonic nor FI losses were measured, and effects of crystal quality in losses could not be separated from the effect of mixing. In our work, we are uniquely able to separate and quantify each of these effects for the first time and find that while necessary for high performance, neither aggregation nor crystallinity correlates well with charge generation, recombination, or performance, especially at low levels of DIO where crystallinity, aggregation, and domain purity are separable.

Our result indicates that donor–acceptor interfaces between pure, aggregated domains are the key to efficient generation. It appears that once some level of aggregation is established, maximizing the purity of the domains (and therefore the probability that interfaces are proximate to aggregates) enables further performance enhancements that go beyond aggregation alone. Recent temperature-dependent measurements on this system have indicated that the energy barrier to charge separation decreases with increasing fullerene aggregation.[14] We posit that this barrier is the cause of FD geminate losses, and increased domain purity increases the proximity of aggregates to the interface, reducing this barrier and the FD geminate losses it causes. Our findings then indicate that further development of highly crystallizing molecular donors and acceptors with a high driving force for phase separation during processing (limited to tens of nanometers in size) will decrease geminate losses, resulting in increasingly efficient solar cell devices. Elimination of this barrier has been reported recently in a high-performing NFA system PM6:Y6;[24] however, FI geminate losses remain, and we establish the PCPDTBT:$PC_{71}BM$ system investigated here as a model system of interest to resolve the mechanism for eliminating such FI losses in NFA systems.

In summary, we demonstrate that our holistic loss analysis for OPVs is capable of separating and quantifying each fundamental loss mechanism within a working device. Surprisingly, unlike P3HT:PCBM and most high-performance systems, we find no measurable field-independent geminate losses in PCPDTBT:PCBM devices. Instead, we find a strong, quantitative correlation between domain purity and field-dependent geminate recombination with an increasing amount of DIO processing additive. We show that, although related, the aggregation and crystallinity are not sufficient to explain the performance trends or the underlying fundamental dynamics. Combined with our previous work, this adds to the evidence of a causal relationship between domain purity and charge generation in all types of organic solar cells and indicates that new molecule design and device processing strategies should target highly crystalline and phase-separated morphologies for continued progress in OPV performance.

METHODS

Device Preparation and Performance. For devices, patterned ITO on glass substrates [145(10) nm, 20(2) Ω square, 88% trans at 550 nm, NIST mask 550 (Thin Film Devices)] was sequentially sonicated in detergent, DI water, acetone, and isopropyl alcohol with a subsequent 15 min UV–ozone treatment. PEDOT:PSS (Clevios P VP AI 4083, Heraeus) hole transport layers were spin-coated onto the substrates. Devices were then transferred into a nitrogen glovebox (O_2 and H_2O at ~0.1 ppm) for the remainder of fabrication and device testing (separate gloveboxes). Active layer chlorobenzene (99% anhydrous, Aldrich) solutions were composed of blends of the copolymer poly[2,6-(4,4-bis(2-ethylhexyl)-4*H*-cyclopenta-[2,1-*b*;3,4-*b*′]dithiophene)-*alt*-4,7-(2,1,3-benzothiadiazole)] (PCPDTBT, 1-Material) and fullerene phenyl-C71-butyric acid methyl ester ($PC_{71}BM$, Nano-C) in a 1:3 ratio. DIO (Aldrich) progressively displaced the host solvent from 0 to 5 vol %. The resulting solutions were heated to 40 °C for at least 10 h to ensure the materials were fully dissolved. Active layers

https://dx.doi.org/10.1021/acs.jpclett.0c03863
J. Phys. Chem. Lett. 2021, 12, 1847–1853

were spin-cast for 60 s at varying spin speeds to first find the optimum performance and then yield a consistent thickness for the rest of the DIO series. Immediately after spin-coating, all fresh active layers were transferred to a vacuum chamber (base pressure of 5×10^{-7} Torr) first to outgas for at least 8 h and then for electrode deposition via thermal evaporation without breaking vacuum (10 nm Ca at 0.4 A/s then 200 nm Al at 1 A/s, NexDep Angstrom Engineering). Each substrate resulted in four symmetric devices with areas of 4 mm^2 with separate anode and cathode traces. JV characterization (Keithley 2450) was conducted under 1 sun conditions (Oriel 300 W xenon lamp with an AM1.5G filter) at 1000 W/m^2 calibrated with a NIST-calibrated silicon photodiode (Thorlabs). All performance parameters reported are averaged from four devices on a single substrate to ensure consistency and reproducibility.

Spectroscopies. UV−vis absorption spectroscopy was carried out on active layers next to devices after electrode deposition. Reference pure films of PCPDTBT were spin-cast on PEDOT:PSS-coated glass substrates following the same steps as for active layer deposition. All optical spectroscopy was performed with an Ocean Optics QEpro spectrometer cooled to −25 °C. For absorption spectroscopy, a lens collimated the fiber-coupled output of a stabilized tungsten−halogen light source (ThorLabs SLS201L) through the sample and into a 0.5 in. fiber-coupling lens for spectrometer measurement. A PEDOT:PSS-coated ITO substrate was used for the incident intensity in Beer's law (base 10) absorbance calculation.

PL excitation was conducted at a wavelength of 600 nm (Ekspla NT232), which balances absorption between the polymer and fullerene. A 690 nm short-pass filter was placed before the sample to remove idler laser light, and a 710 nm long-pass filter was placed after the sample to block the laser signal from the spectrometer. PL was captured via a carefully aligned lens into the Ocean Optics spectrometer.

Time-Delayed Collection Field. Immediately after the JV characterization and on the same probe station in the glovebox, TDCF was conducted for the device with the highest PCE. Pump excitation was at 600 nm due to the balance of polymer and fullerene absorption using an ND-YAG-pumped OPO device (3 ns pulse width running at 100 Hz, Ekspla NT232). A low fluence of only 100 nJ/cm^2 was used along with a 5 ns delay in applying the collection (sweep out) voltage to ensure all generated charges were collected. The collection voltage was applied using a custom-made amplification circuit synchronized with the pump light using a 250 MHz bandwidth function generator (Tektronix AFG 3251). A unique overpulse method was employed to overcome the RC time constant of the device, which can cause field dependence in collected charge even when generated charge is field-independent.[21] Our method initially applies a high voltage across the ITO traces to more quickly build up the internal electric field across the active layer over a time not limited by the device RC time constant. This significantly decreases collection times and, in concert with a low fluence and a short time delay, reduces bimolecular losses and increases the accuracy of TDCF measurement of generation currents over previous studies. The transient photocurrents are measured using a 12-bit, 1 GHz bandwidth oscilloscope (Teledyne LeCroy HDO 4104).

X-ray Scattering. RSoXS was conducted in transmission scattering mode at beamline 11.0.1.2 of the Advanced Light Source.[29] Active layers of the devices tested were transferred to SiN windows (100 nm thick, 2 mm long, Norcada) by dissolving the PEDOT:PSS layer beneath in DI water. The incident beam intensity was calibrated every other sample to reduce possible effects of beam intensity drifting. For RSoXS, data were reduced to one-dimensional profiles using a custom skin[30] on NIKA by Jan Ilavsky[31] in the Igor Pro 8 software platform. An enhanced Q range was attained by acquiring scattering patterns at multiple sample−detector distances.

GIWAXS was conducted at beamline 7.3.3 of the Advanced Light Source.[32] To keep diffraction intensities linear with scattering volume, scattering was acquired at an incident angle of 0.2° (above all critical angles). Scattering patterns were reduced in NIKA and analyzed in Igor Pro 8 using the built-in multipeak fitting program.

■ ASSOCIATED CONTENT

Supporting Information

The Supporting Information is available free of charge at https://pubs.acs.org/doi/10.1021/acs.jpclett.0c03863.

Detailed calculations and more in-depth figures of the data, including OPV performance metrics (SI Note 1), calculation of the maximum current (SI Note 2), transfer matrix methods for calculating active layer absorption (SI Note 3), calculation of transition efficiencies and loss currents (SI Note 4), and GIWAXS analysis of crystallinity (SI Note 5) (PDF)

■ AUTHOR INFORMATION

Corresponding Author

Brian A. Collins − *Department of Physics and Astronomy and Materials Science and Engineering Program, Washington State University, Pullman, Washington 99164, United States;* orcid.org/0000-0003-2047-8418; Email: brian.collins@wsu.edu

Authors

Prabodh Dhakal − *Department of Physics and Astronomy, Washington State University, Pullman, Washington 99164, United States;* orcid.org/0000-0002-5914-0038

Thomas Ferron − *Department of Physics and Astronomy, Washington State University, Pullman, Washington 99164, United States*

Awwad Alotaibi − *Materials Science and Engineering Program, Washington State University, Pullman, Washington 99164, United States*

Victor Murcia − *Materials Science and Engineering Program, Washington State University, Pullman, Washington 99164, United States*

Obaid Alqahtani − *Materials Science and Engineering Program, Washington State University, Pullman, Washington 99164, United States; Department of Physics, Prince Sattam bin Abdulaziz University, Alkharj 11942, Kingdom of Saudi Arabia*

Complete contact information is available at: https://pubs.acs.org/10.1021/acs.jpclett.0c03863

Notes

The authors declare no competing financial interest.

■ ACKNOWLEDGMENTS

Financial support was provided by the National Science Foundation under Grant DMR-1905790. T.F. was supported by the U.S. Department of Energy (DOE) Office of Science, Basic Energy Sciences, Early Career Research Award DE-

SC0017923. This research used resources of the Advanced Light Source, which is a DOE Office of Science User facility operated under Contract DE-AC02-05CH11231.

REFERENCES

(1) Liu, Q.; Jiang, Y.; Jin, K.; Qin, J.; Xu, J.; Li, W.; Xiong, J.; Liu, J.; Xiao, Z.; Sun, K.; Yang, S.; Zhang, X.; Ding, L. 18% Efficiency organic solar cells. *Sci. Bull.* **2020**, *65*, 272−275.

(2) Lin, Y.; Nugraha, M. I.; Firdaus, Y.; Scaccabarozzi, A. D.; Aniés, F.; Emwas, A. H.; Yengel, E.; Zheng, X.; Liu, J.; Wahyudi, W.; Yarali, E.; Faber, H.; Bakr, O. M.; Tsetseris, L.; Heeney, M.; Anthopoulos, T. D. A Simple n-Dopant Derived from Diquat Boosts the Efficiency of Organic Solar Cells to 18.3%. *ACS Energy Lett.* **2020**, *5*, 3663−3671.

(3) Alqahtani, O.; Babics, M.; Gorenflot, J.; Savikhin, V.; Ferron, T.; Balawi, A. H.; Paulke, A.; Kan, Z.; Pope, M.; Clulow, A. J.; Wolf, J.; Burn, P. L.; Gentle, I. R.; Neher, D.; Toney, M. F.; Laquai, F.; Beaujuge, P. M.; Collins, B. A. Mixed Domains Enhance Charge Generation and Extraction in Bulk-Heterojunction Solar Cells with Small-Molecule Donors. *Adv. Energy Mater.* **2018**, *8*, 1702941.

(4) Scarongella, M.; De Jonghe-Risse, J.; Buchaca-Domingo, E.; Causa, M.; Fei, Z.; Heeney, M.; Moser, J. E.; Stingelin, N.; Banerji, N. A close look at charge generation in polymer: Fullerene blends with microstructure control. *J. Am. Chem. Soc.* **2015**, *137*, 2908−2918.

(5) Buchaca-Domingo, E.; Ferguson, A. J.; Jamieson, F. C.; McCarthy-Ward, T.; Shoaee, S.; Tumbleston, J. R.; Reid, O. G.; Yu, L.; Madec, M.-B. B.; Pfannmöller, M.; Hermerschmidt, F.; Schröder, R. R.; Watkins, S. E.; Kopidakis, N.; Portale, G.; Amassian, A.; Heeney, M.; Ade, H.; Rumbles, G.; Durrant, J. R.; Stingelin, N. Additive-assisted supramolecular manipulation of polymer:fullerene blend phase morphologies and its influence on photophysical processes. *Mater. Horiz.* **2014**, *1*, 270−279.

(6) Athanasopoulos, S.; Bässler, H.; Köhler, A. Disorder vs Delocalization: Which Is More Advantageous for High-Efficiency Organic Solar Cells? *J. Phys. Chem. Lett.* **2019**, *10*, 7107−7112.

(7) Bakulin, A. A.; Rao, A.; Pavelyev, V. G.; van Loosdrecht, P. H. M.; Pshenichnikov, M. S.; Niedzialek, D.; Cornil, J.; Beljonne, D.; Friend, R. H. The Role of Driving Energy and Delocalized States for Charge Separation in Organic Semiconductors. *Science* **2012**, *335*, 1340.

(8) Ye, L.; Hu, H.; Ghasemi, M.; Wang, T.; Collins, B. A.; Kim, J. H.; Jiang, K.; Carpenter, J. H.; Li, H.; Li, Z.; McAfee, T.; Zhao, J.; Chen, X.; Lai, J. L. Y.; Ma, T.; Bredas, J. L.; Yan, H.; Ade, H. Quantitative relations between interaction parameter, miscibility and function in organic solar cells. *Nat. Mater.* **2018**, *17*, 253−260.

(9) Lenes, M.; Morana, M.; Brabec, C. J.; Blom, P. W. M. Recombination-limited photocurrents in low bandgap polymer/fullerene solar cells. *Adv. Funct. Mater.* **2009**, *19*, 1106−1111.

(10) Jamieson, F. C.; Agostinelli, T.; Azimi, H.; Nelson, J.; Durrant, J. R. Field-independent charge photogeneration in PCPDTBT/PC70BM solar cells. *J. Phys. Chem. Lett.* **2010**, *1*, 3306−3310.

(11) Gorenflot, J.; Paulke, A.; Piersimoni, F.; Wolf, J.; Kan, Z.; Cruciani, F.; El Labban, A.; Neher, D.; Beaujuge, P. M.; Laquai, F. From Recombination Dynamics to Device Performance: Quantifying the Efficiency of Exciton Dissociation, Charge Separation, and Extraction in Bulk Heterojunction Solar Cells with Fluorine-Substituted Polymer Donors. *Adv. Energy Mater.* **2018**, *8*, 1701678.

(12) Etzold, F.; Howard, I. A.; Forler, N.; Cho, D. M.; Meister, M.; Mangold, H.; Shu, J.; Hansen, M. R.; Müllen, K.; Laquai, F. The effect of solvent additives on morphology and excited-state dynamics in PCPDTBT:PCBM photovoltaic blends. *J. Am. Chem. Soc.* **2012**, *134*, 10569−10583.

(13) Ferron, T.; Waldrip, M.; Pope, M.; Collins, B. A. Increased charge transfer state separation via reduced mixed phase interface in polymer solar cells. *J. Mater. Chem. A* **2019**, *7*, 4536−4548.

(14) Kurpiers, J.; Ferron, T.; Roland, S.; Jakoby, M.; Thiede, T.; Jaiser, F.; Albrecht, S.; Janietz, S.; Collins, B. A.; Howard, I. A.; Neher, D. Probing the pathways of free charge generation in organic bulk heterojunction solar cells. *Nat. Commun.* **2018**, *9*, 2038.

(15) Albrecht, S.; Schindler, W.; Kurpiers, J.; Kniepert, J.; Blakesley, J. C.; Dumsch, I.; Allard, S.; Fostiropoulos, K.; Scherf, U.; Neher, D. of Solvent Additives. *J. Phys. Chem. Lett.* **2012**, *3*, 640.

(16) Kniepert, J.; Schubert, M.; Blakesley, J.; Neher, D. Photogeneration and Recombination in P3HT: PCBM Solar Cells Probed by Time Delayed Collection Field Experiments. *J. Phys. Chem. Lett.* **2011**, *2*, 700−705.

(17) Albrecht, S.; Janietz, S.; Schindler, W.; Frisch, J.; Kurpiers, J.; Kniepert, J.; Inal, S.; Pingel, P.; Fostiropoulos, K.; Koch, N.; Neher, D. Fluorinated Copolymer PCPDTBT with Enhanced Open-Circuit Voltage and Reduced Recombination for Highly Efficient Polymer Solar Cells. *J. Am. Chem. Soc.* **2012**, *134*, 14932.

(18) Albrecht, S.; Tumbleston, J. R.; Janietz, S.; Dumsch, I.; Allard, S.; Scherf, U.; Ade, H.; Neher, D. Quantifying Charge Extraction in Organic Solar Cells: The Case of Fluorinated PCPDTBT. *J. Phys. Chem. Lett.* **2014**, *5*, 1131.

(19) Jain, N.; Chandrasekaran, N.; Sadhanala, A.; Friend, R. H.; McNeill, C. R.; Kabra, D. Interfacial disorder in efficient polymer solar cells: The impact of donor molecular structure and solvent additives. *J. Mater. Chem. A* **2017**, *5*, 24749−24757.

(20) Scharsich, C.; Fischer, F. S. U.; Wilma, K.; Hildner, R.; Ludwigs, S.; Köhler, A. Revealing structure formation in PCPDTBT by optical spectroscopy. *J. Polym. Sci., Part B: Polym. Phys.* **2015**, *53*, 1416−1430.

(21) Würfel, U.; Unmüssig, M. Apparent Field-Dependence of the Charge Carrier Generation in Organic Solar Cells as a Result of (Bimolecular) Recombination. *Sol. RRL.* **2018**, *2*, 1800229.

(22) Würfel, U.; Neher, D.; Spies, A.; Albrecht, S. Impact of charge transport on current-voltage characteristics and power-conversion efficiency of organic solar cells. *Nat. Commun.* **2015**, *6*, 6951.

(23) Burkhard, G. F.; Hoke, E. T.; McGehee, M. D. Accounting for interference, scattering, and electrode absorption to make accurate internal quantum efficiency measurements in organic and other thin solar cells. *Adv. Mater.* **2010**, *22*, 3293−3297.

(24) Perdigón-toro, L.; Zhang, H.; Markina, A.; Yuan, J.; Hosseini, S. M.; Wolff, C. M.; Zuo, G.; Stolterfoht, M.; Zou, Y.; Gao, F.; Andrienko, D.; Shoaee, S.; Neher, D. Barrierless Free Charge Generation in the High-Performance PM6: Y6 Bulk Heterojunction Non-Fullerene Solar Cell. *Adv. Mater.* **2020**, *32*, 1906763.

(25) Collins, B. A.; Li, Z.; Tumbleston, J. R.; Gann, E.; Mcneill, C. R.; Ade, H. Absolute Measurement of Domain Composition and Nanoscale Size Distribution Explains Performance in PTB7: PC 71 BM Solar Cells. *Adv. Energy Mater.* **2013**, *3*, 65−74.

(26) Gu, Y.; Wang, C.; Russell, T. P. Multi-length-scale morphologies in PCPDTBT/PCBM bulk-heterojunction solar cells. *Adv. Energy Mater.* **2012**, *2*, 683−690.

(27) Pfannmöller, M.; Flügge, H.; Benner, G.; Wacker, I.; Sommer, C.; Hanselmann, M.; Schmale, S.; Schmidt, H.; Hamprecht, F. A.; Rabe, T.; Kowalsky, W.; Schröder, R. R. Visualizing a homogeneous blend in bulk heterojunction polymer solar cells by analytical electron microscopy. *Nano Lett.* **2011**, *11*, 3099−3107.

(28) Zusan, A.; Vandewal, K.; Allendorf, B.; Hansen, N. H.; Pflaum, J.; Salleo, A.; Dyakonov, V.; Deibel, C. The crucial influence of fullerene phases on photogeneration in organic bulk geterojunction solar cells. *Adv. Energy Mater.* **2014**, *4*, 1400922.

(29) Gann, E.; Young, A. T.; Collins, B. A.; Yan, H.; Nasiatka, J.; Padmore, H. A.; Ade, H.; Hexemer, A.; Wang, C. Soft x-ray scattering facility at the Advanced Light Source with real-time data processing and analysis. *Rev. Sci. Instrum.* **2012**, *83*, 045110.

(30) Ferron, T.; Collins, B. A. *X-ray Analysis Tools*; 2017 (https://labs.wsu.edu/carbon/xray-analysis-tools/).

(31) Ilavsky, J. Nika: Software for two-dimensional data reduction. *J. Appl. Crystallogr.* **2012**, *45*, 324−328.

(32) Hexemer, A.; Bras, W.; Glossinger, J.; Schaible, E.; Gann, E.; Kirian, R.; MacDowell, A.; Church, M.; Rude, B.; Padmore, H. A SAXS/WAXS/GISAXS beamline with multilayer monochromator. *J. Phys. Conf. Ser.* **2010**, *247*, 012007.

https://dx.doi.org/10.1021/acs.jpclett.0c03863
J. Phys. Chem. Lett. 2021, 12, 1847−1853